Journal of Coordination Chemistry

ISSN: 0095-8972 (Print) 1029-0389 (Online) Journal homepage: http://www.tandfonline.com/loi/gcoo20

Self-assembly and antitumor activity of an organotin coordination polymer containing a helical structure based on copper cyanide and phenanthroline ligand

Safaa El-Din H. Etaiw, Safaa N. Abdou & Abeer A. Faheim

To cite this article: Safaa El-Din H. Etaiw, Safaa N. Abdou & Abeer A. Faheim (2015) Self-assembly and antitumor activity of an organotin coordination polymer containing a helical structure based on copper cyanide and phenanthroline ligand, Journal of Coordination Chemistry, 68:3, 491-506, DOI: 10.1080/00958972.2014.996559

To link to this article: http://dx.doi.org/10.1080/00958972.2014.996559

Accepted author version posted online: 09 Dec 2014.
Published online: 06 Jan 2015.

Journal of Coordination Chemistry, 2015
Vol. 68, No. 3, 491–506, http://dx.doi.org/10.1080/00958972.2014.996559

Self-assembly and antitumor activity of an organotin coordination polymer containing a helical structure based on copper cyanide and phenanthroline ligand

SAFAA EL-DIN H. ETAIW*†, SAFAA N. ABDOU‡ and ABEER A. FAHEIM‡§

†Faculty of Science, Chemistry Department, Tanta University, Tanta, Egypt
‡Faculty of Education and Science (Khourma), Chemistry Department, Taif University, Taif, Saudi Arabia
§Faculty of Science (Girl's), Chemistry Department, Al-Azhar University, Cairo, Egypt

(*Received 30 August 2014; accepted 20 November 2014*)

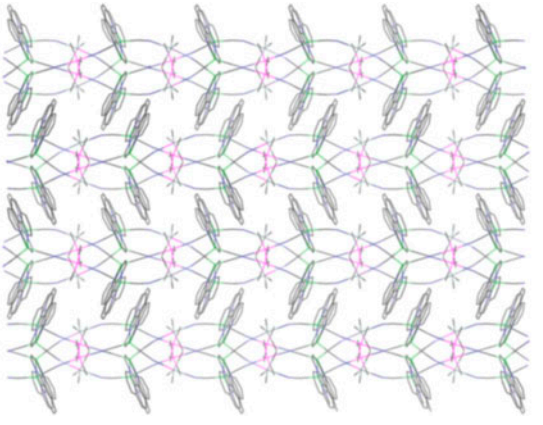

View of the network structure of **1** showing the helical structure of the chains down the projection of the *a*-axis. Hydrogens are omitted for clarity.

A coordination polymer (SCP), $[Cu_2(CN)_4 \cdot (Me_3Sn)_2 \cdot (phen)_2]$, **1**, was constructed based on phenanthroline monohydrated (phen), trimethyltin chloride, and $K_3[Cu(CN)_4]$. The SCP **1** consists of repeating units of tetrahedral $Cu(N_2C_2)$ fragments connected by $(Me_3Sn)^+$ cations which create 1-D helical chains with the phen ligands arranged on both sides of the chain. The 1-D helical chains are arranged in a unique way to form two right-helical and two left-helical chains creating a rare quartet-helical 3-D network. The quartet-helical chains are arranged in a unique A···A···A fashion forming a 3-D network structure via H-bonds and π–π stacking. Mass, electronic and luminescence spectra are also investigated. The MTT assay was used to determine the *in vitro* antitumor effects of SCP **1** on human breast cancer cell line, MCF-7. Cell cycle analysis revealed that SCP **1** induced apoptosis in MCF-7 breast cancer cell line. Thus, the SCP **1** selectivity exhibits specific *in vitro* antitumor effects against human breast cancer cell line, MCF-7.

*Corresponding author. Email: safaaetaiw@hotmail.com

Keywords: Phenanthroline; Trimethyltin chloride; Helical structure; Spectra; Antitumor; Copper cyanide

1. Introduction

Rational design and construction of cyanide-containing coordination polymers is a popular field of research owing to their intriguing molecular topologies and exciting properties [1–11]. A number of cyanide-bridged complexes with intriguing topologies and fascinating properties have been reported, among them cyanide-bridged hetero-metallic complexes [12–17]. [CuCN]-based complexes are subjected to extensive studies, especially in the presence of auxiliary N-donor bridging or chelating ligands [1–5, 18–22]. When N-donor ligands are introduced into [CuCN]-based complexes, the result is a variety of coordination networks. However, to the best of our knowledge, few comprehensive studies of the [CuCN]-based complexes containing organometallic fragments are reported [23–30]. This limited number of structural motifs is known for $[Cu_m(CN)_n\text{-}R_3Sn\text{-}L]$ where L = bipodal organic ligand. This family of organotin polymers was considered as super-Prussian-blue derivatives [31] which are related to zeolites that contain a rod-like anionic $[CN{\cdot}Sn(R_3)\text{-}NC]^-$ nanometer-sized spacer [23–31]. Helical structures have received special attention due to their potential applications in asymmetric catalysis, bioactivity, and nonlinear optical materials [32]. To date, some single- or double-helical chains have been generated [33–40] with most helical polymers being obtained by using chiral ligands [41–44] or oligo-pyridines and other optically active ligands.

Annually, an estimated 10 million people worldwide are diagnosed with cancer, while approximately 6.2 million die from cancer [45]. Among the different kinds of cancer, breast cancer is considered as a major health problem worldwide, affecting 1 in 8–12 women. Breast cancer is the most frequent form of cancer in women [46].

Transition-metal-based organometallic compounds with biological activity have been introduced as new potential therapeutics against cancer, HIV, and malaria, and have already found clinical applications as radiopharmaceuticals, as antibiotics, and as new classes of antibacterial agents with potential for clinical development [47–53]. Many of these putative drugs are centered on classical organometallic motifs, e.g. metallocenes [53, 54], metal–arene complexes [55], metal carbonyl, and carbene complexes [56]. Discovery of the antiproliferative and antitumor activity of cisplatin and its derivatives initiated the investigation for the possible therapeutic applications of other metal-based drugs, often organometallic compounds [57–63], and more particularly organotin(IV) compounds [64–69]. Many different metals have minimized side effects associated with the use of platinum compounds as anticancer drugs [60–63]. Organotin(IV) complexes have interesting *in vivo* anticancer activity as new chemotherapy agents [17, 24, 66–69], binding to membrane proteins or glycoproteins, cellular proteins (e.g. to hexokinase, ATPase, acetyl cholinesterase of human erythrocyte membrane, or to skeletal muscle membranes) [70], or directly with DNA [71].

In continuation of our research on the effect of the N-donor ligands on the structure and properties of the organotin polymers containing CuCN-based adducts, we describe the synthesis, crystal structure, and spectral properties of a SCP that contains $[(Cu)_2(CN)_4]$ fragments, $(Me_3Sn)^+$ cations, and phen as an auxiliary ligand. A new and exciting structure is reported, displaying helical network. Phen is a planar ligand that contains a rigid spacer of

phenyl rings and behaves as a single-connected ligand. Also, phen-based investigations involve studies of copper complex-induced DNA cleavage [72, 73] and it exhibits fluorescence and the spectra are modulated by protonation or metal ion complexes [74]. Therefore, a study has also been carried out on electronic absorption and emission spectra as well as on the antitumor activity *in vitro* against human breast cancer cell line, MCF-7.

2. Experimental

2.1. *Materials*

$K_3[Cu(CN)_4]$ was prepared following the literature procedure [31]. Trimethyltin chloride and phenanthroline monohydrated (phen) were purchased from Aldrich and Sigma and used without purification. Acetonitrile was of analytical grade, supplied by Aldrich and was used as received.

2.2. *Synthesis of $[Cu_2(CN)_4{\cdot}(Me_3Sn)_2{\cdot}(phen)_2]$, 1*

A solution of 44 mg (0.155 mM) of $K_3[Cu(CN)_4]$ in 5 mL H_2O was added under gentle stirring to a solution of 95 mg (0.47 mM) of Me_3SnCl and 30 mg (0.155 mM) of phen in 10 mL of acetonitrile. After one week, yellow prismatic crystals started growing from the initially clear solution. After filtration, washing with small quantities of cold H_2O, and acetonitrile, and overnight drying, 93 mg (65.49% referred to $K_3[Cu(CN)_4]$) of yellow prismatic crystals were obtained. Elemental analysis data for **1** ($C_{34}H_{34}N_8Cu_2Sn_2$, M.W. = 918.5) are as follows, Anal. Calcd: C, 44.42; H, 3.70; N, 12.19; Cu, 13.83. Found: C, 44.37; H, 3.65; N, 12.10; Cu, 13.78.

2.3. *Instruments*

Microanalyses (C, H, N) were carried out with a Perkin–Elmer 2400 automatic elemental analyzer, while copper was determined using a Perkin–Elmer 2380 atomic absorption spectrometer. Infrared (IR) spectra were recorded on a Bruker Vector 22 spectrophotometer as KBr disks from 4000 to 400 cm^{-1}. ^1H NMR spectrum was recorded on a Bruker DPX 200 spectrometer using DMSO-d_6 as solvent. Mass spectra were recorded on a Finnigan MAT 8222 by FAB spectrometer. Electronic absorption spectra were measured on a Shimadzu (UV-3101 PC) spectrometer. Fluorescence spectra of solids were carried out using a Perkin–Elmer (LS 50 B) spectrometer at excitation wavelength 290 nm. X-ray diffraction of single crystals was measured using the Kappa CCD Enraf–Nonius FR590 four circle goniometer with graphite monochromated Mo Kα radiation (λ = 0.71073 Å) operated at 20 mA/50 kV.

2.4. *X-ray crystallography and structure determination*

The well-developed crystal of **1** was mounted on glass fibers and measurements were made at 25 ± 2 °C. The structure was solved using direct methods and all of the non-hydrogen atoms were located from the initial solution or from subsequent electron density difference maps during the initial stages of the refinement. After locating all of the non-hydrogen

Table 1. Crystal data and structure refinement parameters of $[Cu_2(CN)_4 \cdot (Me_3Sn)_2 \cdot (phen)_2]$, **1**.

Empirical formula	$C_{34}H_{34}N_8Cu_2Sn_2$
Formula weight (g M^{-1})	919.174
Temperature (K)	298
Wavelength (Å)	0.71073
Crystal system	Monoclinic
Space group	*C2/c*
Unit cell dimension	
a (Å)	20.4632(6)
b (Å)	19.0804(7)
c (Å)	21.2769(7)
α (°)	90.00
β (°)	115.141(2)
γ (°)	90.00
V (Å^3); *Z*	7520.5(4); 8
D_{Calcd} (g cm^{-3})	1.624
F (0 0 0)	3615
Θ-range (°)	2.910–22.465
Reflections collected/unique	8836/2660
R int	0.040
Data/restraints/parameters	2660/0/415
R indices $[I > 3\sigma(I)]$ R^1/wR^2	0.060/0.161
$W = 1/s^2 (Fo^2) + 0.10000 (Fo^2)$	
R indices (all data)	0.122/0.170
Largest difference peak/hole (e Å^{-3})	2.88/−1.26

atoms in the structure, the model was refined against F^2, first using isotropic and finally anisotropic thermal displacement parameters. The positions of the hydrogens were then calculated and refined isotropically and a final cycle of refinements was performed. The crystal data and structure refinement parameters of **1** are listed in table 1.

2.5. *In vitro antitumor activity*

2.5.1. Cell culture. Trypan blue dye exclusion assay was used to determine cell viability on MCF-7 cells [75]. Cells were maintained in RPMI-1640 media (Gibco) supplemented with 10% Fetal Bovine Serum, 100 Units mL^{-1} penicillin, 100 mg mL^{-1} streptomycin, and 2 mM L-glutamine at 37 °C in a 5% CO_2 atmosphere. After 24 h, one plate of the tested cell line was fixed *in situ* with trichloroacetic acid to represent a measurement of the cell population at the time of drug addition. Aliquots of the tested drug, dissolved in DMSO, at different dilutions were added to the appropriate microtiter wells already containing 100 mL of medium, resulting in the required final drug concentrations. Cell viability was determined with 0.1% trypan blue.

2.5.2. Cell proliferation. Cell growth inhibition was analyzed using the MTT assay. This assay quantifies viable cells by observing the reduction of tetrazolium salt, MTT, to formazan crystals by the cells. 2×10^4 cells/well had been cultured overnight on 96-well plates and media containing different concentrations of SCP **1** were added, each concentration in three repetitions.

At the end of treatment, cells were washed with PBS solution. Then, 100 mL of fresh medium and 50 mL from a stock solution of MTT (3 mg mL^{-1} PBS) were added to each well. After a 30 min period, the absorbance of the samples was measured by an Elisa reader at 564 nm. The absorbance data were converted to % cell viability. Wells containing untreated cells served as positive controls. The mean absorbance of the corresponding set of blanks was subtracted from the mean absorbance of wells incubated with each test agent. This value was then divided by the difference between the mean absorbance of the untreated cells and that of the blanks in order to calculate a percent inhibition for each concentration, which caused a 50% reduction during the drug incubation. The mean IC50 is the concentration of agent that reduces cell growth by 50% under the experimental conditions and is the average with SEM from at least three independent determinations.

2.5.3. Enzyme-linked immunosorbent apoptosis assay. Cells were seeded in a 96-well plate at a density 2×10^4 cells/well and incubated for 24 h. Media were changed to media containing the tested drug (100 mM). Cells were then incubated for an extra 24 h. An ELISA assay was performed using Cell Death Detection ELISAPLUS kit (Roche-Applied Science, Indianapolis, USA) that measures histone release from fragmented DNA in apoptosing cells. Briefly, cells were lysed with 200 mL lysis buffer for 30 min at room temperature. The lysate was centrifuged for 10 min and 20 mL of collected supernatant had been incubated with anti-histone biotin and anti-DNA peroxidase at room temperature for 2 h. After washing with incubation buffer three times, 100 mL of substrate solution (2,2-azinodi(3-ethylbenzthiazolin-sulfuric acid)) was added well and incubated for 15–20 min at room temperature. The absorbance was measured using an ELISA reader at 405 nm. Each assay was done in triplicate and standard deviation (SD) was determined.

2.5.4. Flow cytometric analysis. MCF-7 cells were seeded into six-well plates at a density of 6×10^4 cells per well and incubated for 24 h before radiation. Media were changed to media containing various concentrations of SCP **1**. After 24 h, cells were harvested by trypsinization. The cells were washed with PBS and fixed with ice-cold 70% ethanol while vortexing. Finally, the cells were washed and re-suspended in PBS containing 5 mg mL^{-1} RNase A (Sigma, St. Louis, MO, USA) and 50 mg mL^{-1} propidium iodide (Sigma, St. Louis, MO, USA) for analysis. Cell cycle analysis was performed using FAC-Scan Flow Cytometer (Becton Dickson) according to the manufacturer's protocol.

2.5.5. Determination of caspase-3 activities in compound treated cells. Caspase-3 activity was assayed according to manufacturer's protocol (Assay designs, USA). Briefly, 5×10^6 cells were lysed in 100 μL lysis buffer containing 10 mM HEPES, pH 7.4, 2 mM EDTA, 0.1% CHAPS, 5 mM, 350 μg mL^{-1} PMSF, and 5 mM DTT. Cells were homogenized by three cycles of freezing and thawing and then were centrifuged to remove the cellular debris. Each sample was then incubated in buffer containing 10 mM HEPES, pH 7.4, 2 mM EDTA, 0.1% CHAPS, 5 mM EDTA supplemented with Ac-DEVD-AFC for 1 h at room temperature, and, then, the reaction was stopped with 1 N HCl. The absorbance was measured at 405 nm. Each assay was done in triplicate and SD was determined.

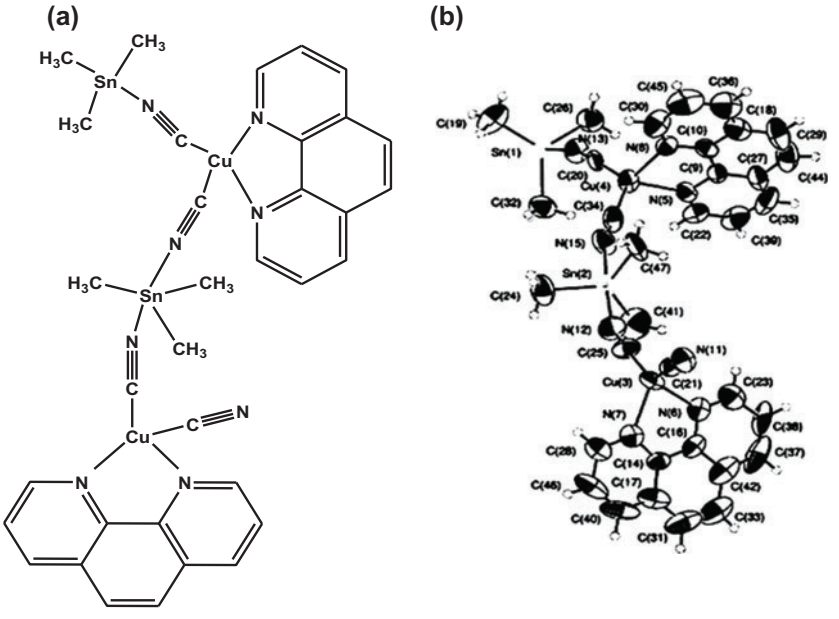

Figure 1. (a) Molecular structure of SCP **1**. (b) An ORTEP view of the asymmetric unit of SCP **1** showing the atom labeling scheme.

Table 2. Selected bond lengths (Å) and angles (°) of **1**.

Sn1–N11	2.286(3)	N6–Cu3–N7	78.88(11)
Sn1–N13	2.368(3)	N6–Cu3–C25	108.07(11)
Sn2–N12	2.362(3)	N7–Cu3–C25	120.30(12)
Sn2–N15	2.273(3)	N6–Cu3–C21	108.93(10)
Cu3–N6	2.126(2)	N7–Cu3–C21	104.76(10)
Cu3–N7	2.135(3)	N5–Cu4–C20	106.71(10)
Cu3–C21	1.906(3)	N8–Cu4–C20	118.70(10)
Cu3–C25	1.896(4)	N5–Cu4–C34	111.13(11)
Cu4–N5	2.127(2)	N8–Cu4–C34	105.18(11)
Cu4–N8	2.116(2)	Cu3–C25–N12	176.8(3)
Cu4–C20	1.898(3)	Cu3–C21–N11	176.9(3)
Cu4–C34	1.915(4)	Cu4–C20–N13	173.6(2)
N11–C21	1.158(3)	Cu4–C34–N15	179.0(3)
N12–C25	1.170(4)	Sn1–N11–C21	168.3(3)
N13–C20	1.151(3)	Sn1–N13–C20	162.7(2)
N15–C34	1.160(3)	Sn2–N12–C25	161.2(3)
N12–Sn2–N15	175.36(9)	Sn2–N15–C34	163.2(3)
N11–Sn1–N13	175.58(8)		

2.5.6. Statistical analysis. Data were expressed as mean ± SD unless otherwise indicated. Statistical differences between the treatment and control groups were calculated with SPSS 12.0 (SPSS, USA). $p < 0.05$ was considered statistically significant.

3. Results and discussion

3.1. *Structure of $[Cu_2(CN)_4{\cdot}(Me_3Sn)_2{\cdot}(phen)_2]$, 1*

The asymmetric unit of **1** is shown in figure 1. It crystallizes in the monoclinic space group *C2/c*. It has two crystallographically independent Cu(I) centers, four cyanides, two $(Me_3Sn)^+$ cations, and two phen ligands per asymmetric unit. In the anionic fragment $\{[Cu_2(CN)_4]^{2-}\}_n$, Cu3 and Cu4 ions have tetrahedral geometry, and thus monovalent. Their coordination polyhedra are defined by two μ^2-bridging cyanide ligands (Cu-C/*N*) [1.896(4)–1.915(4) Å], table 2. The other two coordinating sites are occupied by two nitrogens of phen (Cu-N/phen) [2.116(2)–2.135(4) Å]. All the cyanide groups in $\{[Cu_2(CN)_4]^{2-}\}_n$ are ordered. The copper cyanide angles exhibit bent structure (l25.86–126.2°). The tin has TBPY-5 geometry where the three methyl groups orient toward the corners of a distorted TP-3, table 2. The nitrogens of the cyanide groups occupy axial positions which exhibit nearly right angles; 89.40°, with respect to the Me_3Sn plane. However, the N(11)–Sn(l)–N (13) angle is 175.26° which reflects a bent structure of the (CN–Me_3Sn–NC) connecting unit and the fact that the methyl groups occupy perpendicular positions out of the plane defined by CN–Sn–NC spacer. The structure of **1** consists of repeating units of the tetrahedral $Cu(N_2C_2)$ fragments connected by the $(Me_3Sn)^+$ cations. 1-D helical chains create with the phen ligands arranged on both sides of each chain. The two phen ligands exhibit dihedral angle of 48.50°. The 1-D helical chains are arranged in a unique way to construct two right-helical and two left-helical chains creating a quartet-helical 3-D network, figure 2. The quartet-helical chains are arranged in a unique A···A···A fashion along the *c*-axis with a separation distance of 14.421 Å. On the other hand, the interlayer distance between 2-D sheets along the *b*-axis is 9.221 Å. The quartet-helical chains form a 3-D network structure

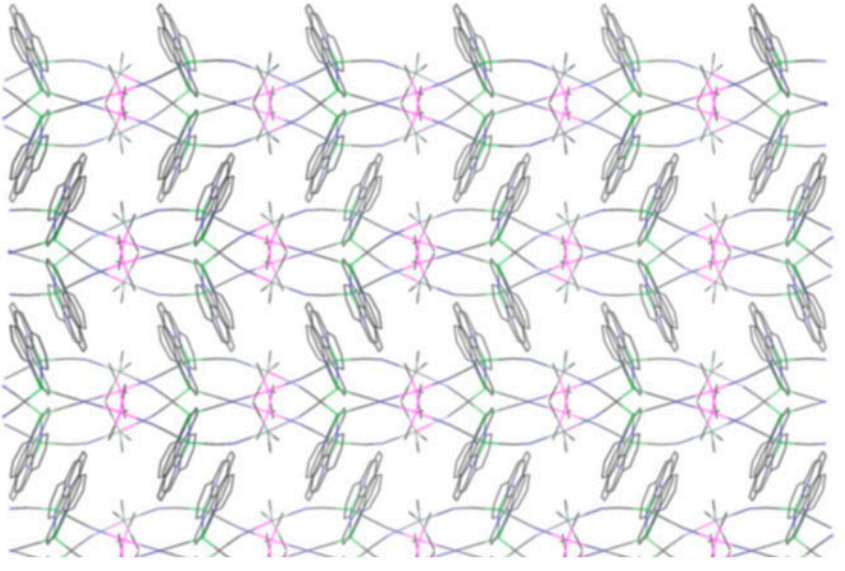

Figure 2. View of the network structure of **1** showing the helical structure of the chains down the projection of the *a*-axis. Hydrogens are omitted for clarity.

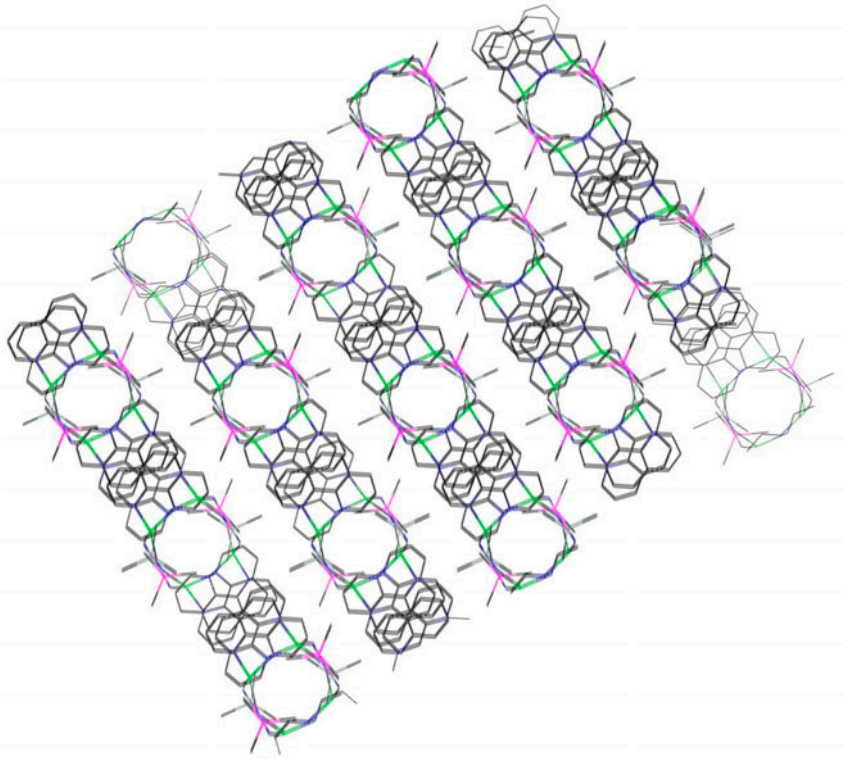

Figure 3. Visualization of the voids and the methyl groups located in the space between the parallel rows in the 3-D network structure of SCP **1** down the projection of the *b*-axis. Hydrogens are omitted for clarity.

via H-bonds (2.305–2.846 Å) and π–π stacking (3.376 Å). Hydrogens of the methyl and phen ligands play an important role in the structure of **1** via H-bonds with C, N, Sn, and Cu. Alternatively, the structure of **1** consists of fascinating blocks along the *b*-axis which contain wide voids with dimensions of 10.713–27.033 Å, figure 3.

Structures of the self-assembly of $[Cu(CN)_4]^{3-}$, $(R_3Sn)^+$, and the auxiliary ligand (L) to form 3-D-SCP, $[Cu(CN)_2(Me_3Sn)(0.5\ bpy)]$ [26], $[Cu(CN)_2(Me_3Sn)pyz]$ [27], $[Cu(CN)_2(Me_3Sn)(0.5\ bpe)]$ [28], $[Cu(CN)_2(Me_3Sn)(0.5\ bpeH_2)]$ [28], $[Cu(CN)_2(Me_3Sn)(cpy)]$ [28], $[Cu_2(CN)_3(Me_3Sn)(qox)]$ [25], $[Cu_2(CN)_4(Ph_3Sn)_2(qox)]$ [76], $[Cu(CN)_2(Me_3Sn)(qaz)]$ [31], where bpy = 4,4′-bipyridine, pyz = pyrazine, bpe = bis(4-pyridyl)-trans-ethene, $bpeH_2$ = bis(4-pyridyl)-1,2-ethane, cpy = 4-cyanopyridine, qox = quinoxaline and qaz = quinazoline, indicate that they exhibit diverse topologies containing different building blocks; $[(Cu(CN)_2]^-$, $[Cu_2(CN)_3]^-$, and $[(Cu_2(CN)_4]^{2-}$ depending on the types of the ligands L and R. None of the structures of these SCP contain the $[Cu(CN)_4]^{3-}$ anion present in $K_3[Cu(CN)_4]$. Also, the crystal structures of these SCP contain L not as a guest, but as a ligand coordinated to Cu(I) which in most cases is a μ^2-bridge. The structure of **1** differs from the structures of these polymers with its unique helical structure and the phen ligands arranged on both sides of the chain. The encapsulation of uncharged or ionic guests (i.e. templates) into the cavities of the CuCN SCP containing (R_3Sn) fragments has attracted

much interest in order to reduce or even to fully exclude lattice interpenetration. The structure of **1** represents an example of an open framework containing wide channels between the helical chains which are occupied by phen ligands.

3.2. *Spectroscopic properties of SCP 1*

The IR spectra of SCP **1** and that of phen indicate the presence of phen, Me_3Sn, and CuCN fragments. The spectrum of **1** displays bands of phen at 3043, 3003 cm^{-1} (υCH(arom)), 1418 cm^{-1} (δCH), and at 784, 726 cm^{-1} (γCH). These bands are shifted to lower wavenumbers from the vibration frequencies of free phen due to formation of hydrogen bonds between hydrogens of the ligand and the donor sites of the (CuCN) fragments. In contrast, the band at 1622 cm^{-1} corresponds to υC=N while those at 1587, 1504, and 1443 cm^{-1} are attributed to υC=C of phen ligand in SCP **1**. These bands exhibit small shifts to lower wavenumbers from those of phen ligand supporting coordination of phen to Cu centers. In consequence of bridging tetrahedral $Cu[N_{2(}phen_{)}(CN)_2]$ building blocks by the Me_3Sn units via a covalent Cu–CN→Sn bond, one can realize the presence of υCN band (2111, 2090 cm^{-1}) at higher wavenumbers than the band of the genuine salt of the corresponding $[Cu(CN)_4]^{3-}$ anion (2076 cm^{-1}) [77], which contains non-bridged cyanide groups. In addition, stretching frequencies much higher than those of the genuine salts, $K_3[Cu(CN)_4]$ and $[(nBu_4N)_3Cu(CN)_4]$ have been assigned to linear bridging between metal centers, while frequencies near those of the salts are associated with terminal or non-linear bridging CN groups [78–80]. The presence of two cyanide bands indicates the presence of two types of cyanide ligands affected by hydrogen bonding. The broad band at 541 cm^{-1} due to asymmetric υSn–C indicates the presence of trigonal plane Me_3Sn units owing to their axial anchoring to two cyanide nitrogens. The υCu–C band at 442 cm^{-1} confirms the presence of the (CuCN) fragments.

The ^{1}H NMR spectrum of **1** shows four broad peaks at 7.11, 8.01, 8.08, and 8.69 ppm corresponding to aromatic protons of phen. This assignment was supported by the ^{1}H NMR spectrum of free phen which exhibits sharp and broad peaks at 7.26, 7.55, 8.0, and 8.81 ppm corresponding to H(2,7), H(4,5), H(3,6), and H(1,8), respectively. The shift in peaks supports the participation of phen in coordination of copper and the formation of H-bonding. Also, ^{1}H-NMR spectrum of **1** shows one singlet for Me_3Sn protons at 0.44 ppm which exhibits two satellite peaks at 0.26 and 0.61 ppm that arise from coupling to ^{117}Sn and ^{119}Sn nuclei [79]. The presence of these satellite peaks are good indication for the presence of Me_3Sn connecting units exhibiting TBPY-5 configuration.

The FAB^+ mass spectrum of **1** exhibits the base peak at *m/z* 165 corresponding to Me_3Sn^+ isotopomer of the molecular ion. The mass spectrum exhibits the molecular ion peak at $m/z = 920$ corresponding to $[M^+]$. The most important ion peak appears at $m/z = 460$ corresponding to $[Cu(CN)_2Me_3Sn(phen)]^+$ which supports the participation of phen and $(Me_3Sn)^+$ in the formation of the network structure of **1**. The ESI^- mass spectrum of **1** displays more than eleven peaks of $[Cu_n(CN)_{n+1}]^-$ units, where the base peak observed at $m/z = 564$ corresponds to $[Cu_6(CN)_7]^-$ isotopomer of the molecular ion, indicating the polymeric nature of the $Cu(CN)_2$ building blocks. The mass spectra indicate the presence of phen, Me_3Sn, and CuCN units. Also, they support the polymeric nature of the $Cu(CN)_2$ building blocks.

3.3. *Electronic absorption and emission spectra of SCP 1*

The electronic absorption spectrum of 1, 10-phenanthroline resembles the spectra of phenanthrene and anthracene and, consequently, that of naphthalene. Substitution of nitrogen for methane in 1, 10-phenanthroline, just as in naphthalene, produces only relatively small spectroscopic changes, table 3. The short wavelength band in phenanthroline, with a peak at 200 nm, is assigned to the $^1B_a \leftarrow {}^1A$ transition. The longitudinally polarized $^1B_b \leftarrow {}^1A$ band at 225 nm resembles that observed in the spectrum of phenanthrene at 221 nm [81]. The broad band at 260 nm can be considered as a composite one, since the ^1L_b band was submerged under the ^1L_a band like the case of anthracene [81]. This band exhibits more blue shift than that observed in the spectra of naphthalene (286 nm) and anthracene (310 nm) [81]. Thus, this broad band can be assigned to $^1L_a \leftarrow {}^1A$ and $^1L_b \leftarrow {}^1A$ transitions. The last long wavelength band at 285 nm is weak and corresponds to n–π^* transition which disappears on the addition of HCl.

The spectrum of SCP **1** displays the same bands of phenanthroline at more or less the same positions, table 3, except the n–π^* band which disappears indicating participation of phenanthroline in the coordination sphere of copper. Unmodified phen is a weakly emissive compound but, following several routes, a wide range of highly luminescent phenanthroline compounds with emission bands ranging from the UV to the near infrared region can be obtained [82]. Phenanthroline exhibits close π–π^* and n–π^* singlet excited states and the emission originates mainly from the former [82]. Excited states n–π^* often decay via non-radiative pathways, and they are usually characterized by vanishingly low emission quantum yields. Phenanthroline itself is characterized by a weak fluorescence quantum yield ($\Phi_{fl} = 0.0087$) and a short singlet lifetime ($t < 1$ ns) at room temperature [83]. The emission spectrum of phen in DMF displays a well-developed band at 380 nm and a shoulder at 480, table 3 and figure 4. The first band corresponds to the π–π^* transition. The low-energy, delayed emission band at 430 nm can be assigned to the triplet excimer phosphorescence of phen. This assignment was substantiated by reference to the excimer phosphorescence of naphthalene, quinoxaline, and phenanthroline [84].

With respect to the emission spectrum of SCP **1**, it displays a well-developed band at 375 nm and two broad bands at 430 and 480 nm. The structure of SCP **1** contains the CuCN fragment and phen, both of them luminescent at $\lambda_{max} = 390$ nm [85]. The amine-bearing CuCN complexes emit in the visible region while their photophysical behavior appears to be close to that of CuCN itself [86]. The emission spectrum of CuCN is assumed to arise from transition between the lowest triplet excited state and the ground state. It is also supposed that a bent triplet state is responsible for the relatively high energy CuCN

Table 3. Absorption and emission bands (nm) of phen and SCP **1**.

Compound	λ_{abs}	Assignment	λ_{em}	Assignment
Phen	200	$^1B_a \leftarrow {}^1A$	380	Close lying π–π^* transition
	225	$^1B_b \leftarrow {}^1A$	430	Triplet excimer of phen
	260	$(^1L_a \leftarrow {}^1A) + (^1L_b \leftarrow {}^1A)$		
	285	n–π^*		
SCP **1**	202	$^1B_a {}^1A$	375	Close lying π–π^* transition
	228	$^1B_b \leftarrow {}^1A$	430	S_o –T CuCN + triplet excimer of phen
	263	$(^1L_a \leftarrow {}^1A) + (^1L_b \leftarrow {}^1A)$	480	MLCT

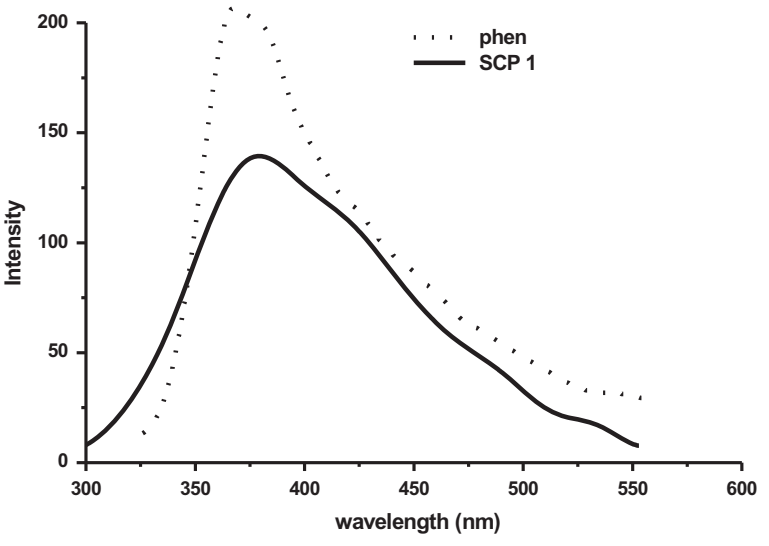

Figure 4. Emission spectra (λ_{ex} = 290 nm) of phen and SCP **1**.

emission [87]. Photophysical properties of phen, as well as that of CuCN, can be tuned by formation of SCP. Thus, the emission band of SCP **1** at 375 nm corresponds to close lying π–π* transition of phen. The broad band at 430 nm can be assigned to the triplet excimer phosphorescence of phen and to So–T transition in the CuCN fragments which suffers a shift to longer wavelength by 40 nm than that of CuCN itself. Thus, the luminescence behavior of phen shows excellent sensitivity towards copper which makes it attractive as a luminescent sensor. The broad, low energy band at 480 nm can be assigned to the metal to ligand charge transfer (MLCT). However, due to the broadening of this band, the possibility exists of single-metal-centered (MC) transitions of the type $3d^{10} \rightarrow 3d^9\ 4s^1$ and $3d^{10} \rightarrow 3d^9\ 4p^1$ on the Cu(I) center.

3.4. *Thermogravimetric analysis of 1*

The TGA curve of **1** shows that the framework of this organotin complex can be intact to 190 °C. On further heating, **1** loses weight from 170 to 620 °C. The first step from 190 to 330 °C corresponds to decomposition of the two phen ligands, Δm% obser. (Calcd) 39.2 (39.1)%. The loss of two molecules of Me_3SnCN occurs in two successive steps between 345 and 490 °C. The relatively high temperature for releasing Me_3SnCN may be due to the helical structure as well as to involving CN and methyl groups in strong H-bonding. The remaining cyanide groups are lost as cyanogen at 510–620 °C, Δm% obser. (Calcd) 11.5 (11.4)%. The weight of the residue obtained after complete thermolysis of **1** is consistent with metallic copper (2Cu)% Δm% obser. (Calcd) 13.8 (13.7)%. These data indicate the stability of the helical chains up to 620 °C.

3.5. *Cytotoxic activity in vitro of SCP 1 on MCF-7 human breast cancer cell line*

Thiazolyl Blue Tetrazolium Bromide (MTT) assay, which serves as an index of cell viability, was conducted to examine *in vitro* cytotoxic activity of SCP **1** against human breast adenocarcinoma cells (MCF-7). Different concentrations of SCP **1** were prepared and dissolved in complete RPMI-1640 media with 10% serum. The results revealed that SCP **1** was able to inhibit the growth of MCF-7 human breast cancer cells in a dose-dependent manner, figure 5. Growth inhibition of 50% (IC50) is calculated as the SCP **1** concentration, which caused a 50% reduction in cell proliferation during the drug incubation. The mean IC50 is the concentration of drug that reduces cell growth by 50% under the experimental conditions and is the average with SEM from at least three independent determinations giving an IC50 value of 1.9 ± 0.3 μM. All in all, the tested SCP **1** at a concentration of IC50 value decreased cell viability of MCF-7 cells compared to the control group.

To examine if SCP **1** has a cytotoxic effect, SCP **1** was tested against non-tumorigenic cell lines derived from breast tissue (MCF10A) *versus* MCF-7 cell line as a positive cancer cell line control, figure 6. The tested SCP **1** showed IC50 > 40(±0.2) μM against MCF10A. These results indicate that the tested SCP **1** showed no cytotoxic effects on normal, non-tumorigenic cell lines derived from breast tissue (MCF10A) compared to MCF-7 breast cancer cells. Taken together, the results confirmed not only the selectivity of the tested SCP **1** that decreased cell viability of MCF-7 breast cancer cells, but also indicated its lower toxicity against normal cells.

3.6. *The SCP 1 induced apoptosis through caspase-3 activation in MCF-7 breast cancer cells*

To investigate if the decrease in cell viability could be due to apoptosis, ELISA assay was performed, which detected histone release from apoptotic cells. The results showed that

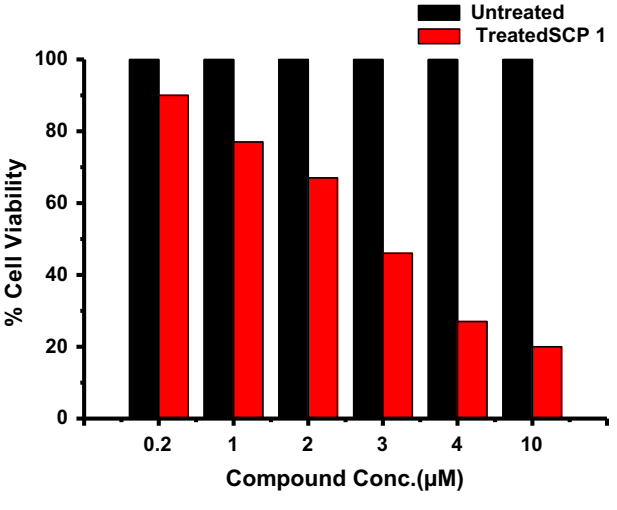

Figure 5. *In vitro* cytotoxicity of SCP **1** against MCF-7 human breast cancer cell lines using different concentrations of the SCP. Untreated cells were used as reference. Each data point is an average of three independent experiments and expressed as M ± SD.

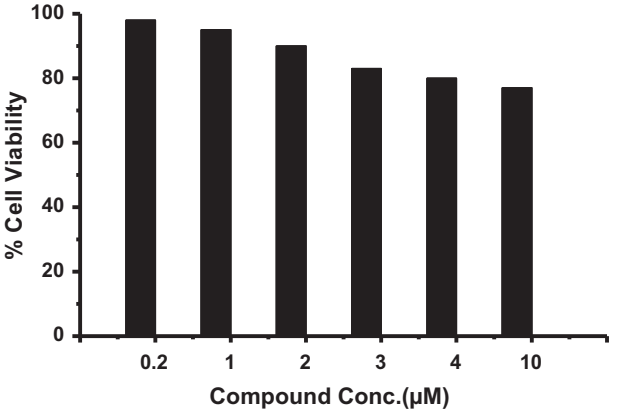

Figure 6. *In vitro* cytotoxicity of SCP **1** against MCF10A, a non-tumorigenic breast epithelial cell line, using different concentrations of the tested compound. Each data point is an average of three independent experiments and expressed as M ± SD.

1.9 μM of the tested SCP **1** induced apoptosis in MCF-7 human breast cancer cells, figure 7. Moreover, the tested SCP **1** showed high % of apoptotic MCF-7 cells compared to control cells cultured in RPMI-1640 media alone. To confirm if the detected decrease in cell viability in the SCP **1** treated MCF-7 cells could be due to apoptosis induction, cell cycle analysis was performed. Figure 8 shows the cell cycle analysis for control and the SCP **1** treated MCF-7 cells. The SCP **1** significantly induced apoptosis in MCF-7 cells with G2 arrest after 24 h of treatment compared to control cells, suggesting that the active SCP **1** induced apoptosis in MCF-7 human breast cancer cells.

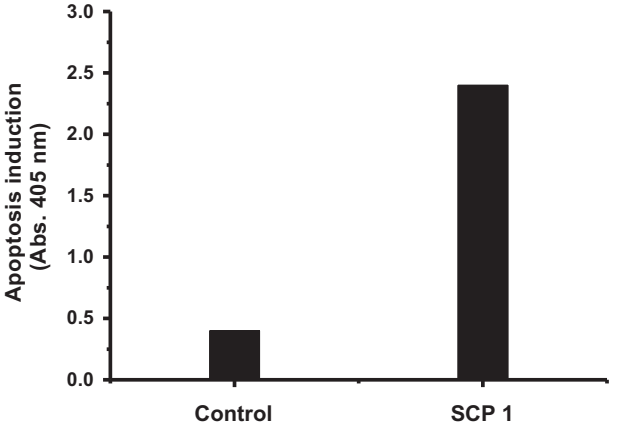

Figure 7. The SCP **1** induced apoptosis in MCF-7 human breast cancer cell lines. ELISA assay was performed to detect apoptotic cells. MCF-7 cells were treated with SCP **1** for 24 h. Cells without drug treatment were used as control, $*p < 0.05$ as compared to untreated control using the unpaired Student *t*-test. Each data point was an average of results from three independent experiments performed in triplicate and presented as M ± SD.

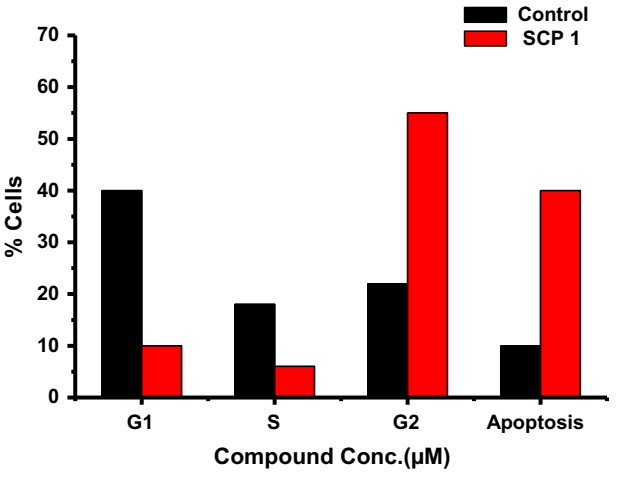

Figure 8. Cell cycle analysis for MCF-7 human breast cancer cells treated with SCP **1**. The % of cell cycle phases was determined in MCF-7 cells treated with or without SCP **1** for 24 h, $*p < 0.05$ as compared to untreated controls using the unpaired Student *t*-test. Each data point was an average of results from three independent experiments performed in triplicate and presented as M ± SD.

4. Conclusion

The new SCP **1** was synthesized to examine the effects on viability and proliferation of MCF-7 human breast cancer cell line. SCP **1** consists of repeating units of the tetrahedral $Cu(N_2C_2)$ fragments connected by $(Me_3Sn)^+$ cations with the phen ligands arranged on both sides of quartet-helical chains which are arranged in a unique A···A···A fashion forming a 3-D network structure via H-bonds and π–π stacking.

SCP **1** shows inhibition of cell viability giving an IC50 value of 1.9 μM, more inhibitory effects than carboplatin (IC50% = 10.5 μM) and Doxorubicin (DOX) (IC50% = 4.35 μM) while close to cisplatin (IC50% = 1.4 μM) [88] on MCF-7 cell line.

The tested SCP **1** has more inhibitory effects against MCF-7 than $[(Ph_3SnCl)_2(bpy)_{1.5}]$, $[(Ph_3SnCl)_2{\cdot}tbpe]$, and $[(Ph_3SnCl)_2{\cdot}bpe]$ which exhibit *in vitro* antitumor activity against human breast cancer cell line, MCF-7 giving an IC50 value of 2.7 μM [89]. On the other hand, the compounds $[Me_3Sn(CH_3C_6H_4SeO_2)]_n$ and $[Ph_3Sn(CH_3C_6H_4SeO_2)]_n$, where $(CH_3C_6H_4SeO_2)$ = 2-methylbenzeneseleninic acid, show significant potency *in vitro* against the SMMC-7721, P388, and MCF-7 cell lines and their antitumor activities are higher than that of cisplatin [90]. However, cytotoxic activities of triorganotin(IV) complexes (R = Ph, Me) decrease in the order Ph > Me. The higher cytotoxic activity of the phenyl derivatives are presumably due to phenyls with high lipophilic character, facilitating binding to biological molecules by $\pi\cdots\pi$ interactions [91].

This study discovered a new class of promising anti-breast cancer agents. Additional experiments *in vitro* and *in vivo* are required to determine the exact mechanism of action of this new SCP that could be a hope to decrease breast cancer invasion and metastasis.

References

[1] S.E.H. Etaiw, A.S. Badr El-din. *J. Inorg. Organomet. Polym.*, **21**, 110 (2011).
[2] S.E.H. Etaiw, T.A. Fayed, S.N. Abdou. *J. Inorg. Organomet. Polym.*, **20**, 326 (2010).
[3] S.E.H. Etaiw, M.M. El-bendary. *J. Inorg. Organomet. Polym.*, **23**, 510 (2013).
[4] S.E.H. Etaiw, M.M. El-bendary. *Spectrochim. Acta, Part A*, **110**, 304 (2013).
[5] S.E.H. Etaiw, M.E. El-Zaria, T.A. Fayed, S.N. Abdou. *J. Inorg. Organomet. Polym.*, **21**, 480 (2011).
[6] E. Chelebaeva, J. Larionova, Y. Guari, R.A. Sá Ferreira, L.D. Carlos, F.A. Almeida Paz, A. Trifonov, C. Guérin. *Inorg. Chem.*, **47**, 775 (2008).
[7] B.A. Maynard, R.E. Sykora, J.T. Mague, A.E.V. Gorden. *Chem. Commun.*, **46**, 4944 (2010).
[8] J. Larionova, Y. Guari, C. Blanc, P. Dieudonne, A. Tokarev, C. Guerin. *Langmuir*, **25**, 1138 (2009).
[9] A.P. Baioni, M. Vidotti, P.A. Fiorito, E.A. Ponzio, S.I.C. de Torresi. *Langmuir*, **23**, 6796 (2007).
[10] J.T. Culp, M.R. Smith, E. Bittner, B. Bockrath. *J. Am. Chem. Soc.*, **130**, 12427 (2008).
[11] S.S. Kaye, J.R. Long. *J. Am. Chem. Soc.*, **127**, 6506 (2005).
[12] A.H. Yuan, R.Q. Lu, H. Zhou, Y.Y. Chen, Y.Z. Li. *Cryst. Eng. Comm.*, **12**, 1382 (2010).
[13] C.C. Zhao, W.W. Ni, J. Tao, A.L. Cui, H.Z. Kou. *Cryst. Eng. Comm.*, **11**, 632 (2009).
[14] Z.Y. Li, N. Wang, J.W. Dai, S.T. Yue, Y.L. Liu. *Cryst. Eng. Comm.*, **11**, 2003 (2009).
[15] A.L. Goodwin, B.J. Kennedy, C.J. Kepert. *J. Am. Chem. Soc.*, **131**, 6334 (2009).
[16] S.E.H. Etaiw, A.S. Badr El-din. *J. Inorg. Organomet. Polym.*, **22**, 478 (2012).
[17] S.E.H. Etaiw, A.S. Sultan, A.S. Badr El-din. *Eur. J. Med. Chem.*, **46**, 5370 (2011).
[18] D.J. Chesnut, D. Plewak, J. Zubieta. *J. Chem. Soc., Dalton Trans.*, 2567 (2001).
[19] S.E.H. Etaiw, S.A. Amer, M.M. El-bendary. *J. Mater. Sci.*, **45**, 1307 (2010).
[20] S.E.H. Etaiw, S.A. Amer, M.M. El-bendary. *Polyhedron*. **28**, 2385 (2009).
[21] S.E.H. Etaiw, M.M. El-bendary. *J. Inorg. Organomet. Polym.*, **20**, 739 (2010).
[22] A.N. Ley, L.E. Dunaway, T.P. Brewster, M.D. Dembo, T.D. Harris, F. Baril-Robert, X. Li, H.H. Patterson, R.D. Pike. *Chem. Commun.*, **46**, 4565 (2010).
[23] S.V. Wegner, H. Arslan, M. Sunbul, J. Yin, C. He. *J. Am. Chem. Soc.*, **132**, 2567 (2010).
[24] S.E.H. Etaiw, A.S. Sultan, M.M. El-bendary. *J. Organomet. Chem.*, **696**, 1668 (2011).
[25] S.E.H. Etaiw, T.A. Fayed, M.B. El-zaria, S.N. Abdou. *J. Inorg. Organomet. Polym.*, **21**, 36 (2011).
[26] A.M.A. Ibrahim, E. Siebel, R.D. Fischer. *Inorg. Chem.*, **37**, 3521 (1998).
[27] E. Siebel, A.M.A. Ibrahim, R.D. Fischer. *Inorg. Chem.*, **38**, 2530 (1999).
[28] H. Hanika-Heidl, S.E.H. Etaiw, M.Sh. Ibrahim, A.S. Badr El-din, R.D. Fischer. *J. Organomet. Chem.*, **684**, 329 (2003).
[29] S.E.H. Etaiw, T.A. Fayed, S.N. Abdou. *J. Organomet. Chem.*, **695**, 1918 (2010).
[30] (a) S.E.H. Etaiw, T.A. Fayed, S.N. Abdou. *J. Inorg. Organomet. Polym.*, **20**, 326 (2010); (b) S.E.H. Etaiw, S.N. Abdou. *J. Inorg. Organomet. Polym.*, **22**, 780 (2012).
[31] E.M. Poll, J.U. Schutze, R.D. Fischer, N.A. Davies, D.C. Apperley, R.K. Harris. *J. Organomet. Chem.*, **621**, 254 (2001).
[32] J.M. Lehn. *Supramolecular Chemistry*, Wiley-VCH, Weinheim (1995).
[33] H.W. Kuai, X.C. Cheng, X.H. Zhu. *Polyhedron*. **50**, 390 (2013).
[34] W.H. Huang, L. Hou, B. Liu, L. Cui, Y.Y. Wang, Q.-Z. Shi. *Inorg. Chim. Acta*. **382**, 13 (2012).
[35] X. He, C.Z. Lu, D.Q. Yuan, S.M. Chen, J.T. Chen. *Eur. J. Inorg. Chem.*, **11**, 2181 (2005).
[36] X. He, C.Z. Lu, C.D. Wu, L.J. Chen. *Eur. J. Inorg. Chem.*, **12**, 2491 (2006).
[37] S. Lopez, S.W. Keller, *Crystal Engineering*, Vol. 2, p. 101, (1999).
[38] C. Piguet, G. Bernardinelli, G. Hopfgartner. *Chem. Rev.*, **97**, 2005 (1997).
[39] F.G. Gelalcha, M. Schulz, R. Kluge, J. Sieler. *J. Chem. Soc., Dalton Trans.*, 2517 (2002).
[40] D. Sun, R. Cao, Y.-Q. Sun, W.-H. Bi, X. Li, M.-C. Hong, Y.-J. Zhao. *Eur. J. Inorg. Chem.*, 38 (2003).
[41] D.L. Reger, R.F. Semeniuc, M.D. Smith. *Eur. J. Inorg. Chem.*, 543 (2002).
[42] J.M. Rowland, M.M. Olmstead, P.K. Mascharak. *Inorg. Chem.*, **41**, 1545 (2002).
[43] C.S.A. Fraser, D.J. Eisler, M.C. Jennings, R.J. Puddephatt. *Chem. Commun.*, 1224 (2002).
[44] G. Jaouen, A. Vessieres, I.S. Butler. *Acc. Chem. Res.*, **26**, 361 (1993).
[45] D.M. Parkin, F. Bray, J. Ferlay, P. Pisani. *Int. J. Cancer*, **94**, 153 (2001).
[46] D.M. Parkin, F. Bray, J. Ferlay, P. Pisani. *CA: Cancer J. Clin.*, **55**, 74 (2005).
[47] K. Severin. *Chem. Commun.*, 3859 (2006).
[48] G. Gasser, N. Metzler-Nolte. *Curr. Opin. Chem. Biol.*, **16**, 84 (2012).
[49] G. Gasser, I. Ott, N. Metzler-Nolte. *J. Med. Chem.*, **54**, 3 (2011).
[50] C. Hartinger, P.J. Dyson. *Chem. Soc. Rev.*, **38**, 391 (2009).
[51] M. Patra, G. Gasser, M. Wenzel, K. Merz, J.E. Bandow, N. Metzler-Nolte. *Organometallics*. **31**, 5760 (2012).
[52] R. Alberto. *J. Organomet. Chem.*, **692**, 1179 (2007).
[53] C. Ornelas. *New J. Chem.*, **35**, 1973 (2011).
[54] G. Erker. *J. Organomet. Chem.*, **692**, 1187 (2007).
[55] W.H. Ang, P.J. Dyson. *Eur. J. Inorg. Chem.*, 4003 (2006).
[56] D.R. van Staveren, N. Metzler-Nolte. *Chem. Rev.*, **104**, 5931 (2004).

[57] G. Sava, G. Jaouen, E.A. Hillard, A. Bergamo. *Dalton Trans.*, **41**, 8226 (2012).
[58] J.M. Hearn, I. Romero-Canelón, B. Qamar, Z. Liu, I. Hands-Portman, P.J. Sadler. *ACS Chem. Biol.*, **8**, 1335 (2013).
[59] A. Hottin, D.W. Wright, A. Steenackers, P. Delannoy, F. Dubar, C. Biot, G.J. Davies, J.-B. Behr. *Chem. Eur. J.*, **19**, 9526 (2013).
[60] M.M. Meier, C. Rajendran, C. Malisi, N.G. Fox, C. Xu, S. Schlee, D.P. Barondeau, B. Höcker, R. Sterner, F.M. Raushel. *J. Am. Chem. Soc.*, **135**, 11670 (2013).
[61] M.A. Jakupec, M. Galanski, V.B. Arion, C.G. Hartinger, B.K. Keppler. *Dalton Trans.*, 183 (2008).
[62] K. Strohfeldt, M. Tacke. *Chem. Soc. Rev.*, **37**, 1174 (2008).
[63] C.G. Hartinger, P.J. Dyson. *Chem. Soc. Rev.*, **38**, 391 (2009).
[64] A.M. Pizarro, A. Habtemariam, P.J. Sadler. *Top Organomet. Chem.*, **32**, 21 (2010).
[65] L. Pellerito, L. Nagy. *Coord. Chem. Rev.*, **224**, 111 (2002).
[66] K. Sotiris Hadjikakou, N. Hadjiliadis. *Coord. Chem. Rev.*, **253**, 235 (2009).
[67] V. Dokorou, A. Primikiri, D. Kovala-Demertzi. *J. Inorg. Biochem.*, **105**, 195 (2011).
[68] D. De Vos, R. Willem, M. Gielen, K.E. Van Wingerden, K. Nooter. *Met-Based Drugs*, **5**, 179 (1998).
[69] M. Gielen, E.R.T. Tiekink. *Tin Compounds and their Therapeutic Potential*. In *Metallotherapeutic Drugs and Metal-based Diagnostic Agents: The Use of Metals in Medicine*, pp. 421–439. M. Gielen and E.R.T. Tiekink (Eds.), Wiley, West Sussex (2005).
[70] L. Pellerito, L. Nagy. *Coord. Chem. Rev.*, **224**, 111 (2002).
[71] M.L. Falcioni, M. Pellei, R. Gabbianelli. *Mutat. Res. Genet. Toxicol. Environ. Mutagen.*, **653**, 57 (2008).
[72] D.R. McMillin, K.M. McNett. *Chem. Rev.*, **98**, 1201 (1998).
[73] K. Hayashi, H. Akutsu, H. Ozaki, H. Sawai. *Chem. Commun.*, 1386 (2004).
[74] (a) H.S. Joshi, R. Jamshidi, Y. Tor. *Angew. Chem.*, **111**, 2888 (1999); (b) H.S. Joshi, R. Jamshidi, Y. Tor. *Angew. Chem. Int. Ed.*, **38**, 2722 (1999).
[75] P. Skehan, R. Storeng, D. Scudiero, A. Monks, J. McMahon, D. Vistica, J.T. Warren, H. Bokesch, S. Kenney, M.R. Boyd. *J. Natl. Cancer Inst.*, **82**, 1107 (1990).
[76] S.E.H. Etaiw, S.N. Abdou. *J. Inorg. Organomet. Polym.*, **20**, 622 (2010).
[77] R.A. Penneman, L.H. Jones. *J. Chem. Phys.*, **24**, 293 (1956).
[78] A.K. Brimah, E. Siebel, R.D. Fischer, N.A. Davies, D. Apperley, R.K. Harris. *J. Organomet. Chem.*, **475**, 85 (1994).
[79] A.M.A. Ibrahim. *J. Organomet. Chem.*, **556**, 1 (1998).
[80] A. Bonardi, C. Carini, C. Pelizzi, G. Pelizzi, G. Predieri, P. Tarasconi. *J. Organomet. Chem.*, **401**, 283 (1991).
[81] H.H. Jalfe', M. Orechin. *Theory and Applications of Ultraviolet Spectroscopy*, 5th Edn, Wiley, New York (1970).
[82] N. Armaroli, L.D. Cola, V. Balzani, J.-P. Sauvage, C. Dietrich-Buchecker, J.-M. Kern. *J. Chem. Soc., Faraday Trans.*, **88**, 553 (1992).
[83] B.N. Bandyopadhyay, A. Harriman. *J. Chem. Soc., Faraday Trans. 1*, **73**, 663 (1977).
[84] G.M. Badger, I.S. Walker. *J. Chem. Soc.*, 122 (1956).
[85] K. Yamamote, T. Takemura, H. Baba. *Bull. Chem. Soc. Jpn.*, **51**, 729 (1978).
[86] M.J. Lim, C.A. Murray, T.A. Tronic, K.E. deKrafft, A.N. Ley, J.C. deButts, R.D. Pike, H. Lu, H.H. Patterson. *Inorg. Chem.*, **47**, 6931 (2008).
[87] C.A. Bayse, T.P. Brewster, R.D. Pike. *Inorg. Chem.*, **48**, 174 (2009).
[88] R. Willem, A. Bouhdid, M. Biesemans, J.C. Martins, D. de Vos, E.R.T. Tiekink, M. Gielen. *J. Organomet. Chem.*, **514**, 203 (1996).
[89] A.S. Badr El-Din, S.E.H. Eaiw, M.E. El-Zaria. *J. Coord. Chem.*, **65**, 3776 (2012).
[90] R.F. Zhang, J. Ru, Z.X. Li, C.L. Ma, J.P. Zhang. *J. Coord. Chem.*, **64**, 4122 (2011).
[91] R.F. Zhang, P.Z. Yan, Q.L. Li, C.L. Ma. *J. Coord. Chem.*, **67**, 649 (2014).